Scanning Tunneling Microscopy Determination of Single Nanocrystal Core Sizes via Correlation with Mass Spectrometry

T. P. Bigioni,[†,‡] T. G. Schaaff,[§] R. B. Wyrwas,[†] L. E. Harrell,[∥,⊥] R. L. Whetten,[†,∥] and P. N. First*[,∥]

School of Chemistry, Georgia Institute of Technology, Atlanta, Georgia 30332-0400, School of Physics, Georgia Institute of Technology, Atlanta, Georgia 30332-0430, and Oak Ridge National Laboratory, Oak Ridge, Tennessee 37831-6365

Received: December 3, 2003

We show that single alkanethiol-passivated gold nanocrystals can be identified by core size in scanning tunneling microscopy (STM) experiments, through a comparison of the measured STM heights with a direct determination of the gold core sizes by mass spectrometry. We take advantage of the discrete size distribution to correlate the peaks in a histogram of nanocrystal heights with the distinct abundance peaks in a mass spectrum. The correlation establishes a mapping from STM height to core mass or mean core diameter. This is vitally important for the interpretation of size-dependent "single-molecule" tunneling spectra from nanocrystal compounds.

1. Introduction

Small gold nanocrystals prepared and isolated via wet-chemical methods have been shown to form a family of giant cluster molecules in the 1−3 nm size range.[1,2] The members are distinct chemical species whose physical properties vary depending on the number of gold atoms and the type of encapsulating ligand. Although gas-phase cluster formation often favors certain cluster sizes over others,[3−5] cluster sizes between these "magic numbers" are still observed as kinetic intermediaries. In a wet chemical synthesis, however, it is possible to produce predominantly the thermodynamically stable products. In particular, etching and subsequent passivation of the gold core may result in the production of discrete, thermodynamically favored cluster molecules.[1,2] However, despite advances in the preparation and isolation (or separation) of these (giant) metal-cluster-compound materials, they have never been conclusively demonstrated to exist as molecularly defined substances, i.e., having one single molecular structure with precise composition and associated properties. Single-molecule imaging and spectroscopy measurements, such as scanning tunneling microscopy and spectroscopy (STM/STS), could elucidate this issue. For instance, direct determination of unique "fingerprint" spectra for each distinct nanocrystal size would be compelling evidence for molecularly defined substances.

Gold nanocrystals with up to ∼200 gold atoms generally do not have bulk crystal structure.[6−8] Because the core structure is not a simple variation of diameter within a bulk lattice framework, the electronic structure is not expected to vary uniformly. Calculations of the density of electronic states in these metal particles show that the spectra should indeed be complex.[9,10] This is in contrast to the smooth variation of spectral features as a function of size observed in semiconductor clusters[11,12] and larger metal clusters.[13] In ensemble measurements of smaller gold nanocrystals (<2 nm diameter) at room temperature, the predicted complex spectra were not fully resolved, but systematic variations of electronic structure were observed with respect to nanocrystal core size.[14]

For comparison to ensemble measurements, and to quantify the evolution of electronic structure, it will be essential to obtain an accurate determination of nanocrystal core size in single-nanocrystal techniques such as STM and STS. One must identify and differentiate between different nanocrystal species and thereby unambiguously attribute each measured spectrum to a particular core size. In principle, this could be accomplished through careful separation of the various nanocrystal species before deposition on a substrate.[15] However, for STS it is far preferable to work with a single sample of mixed sizes so that the tunneling conditions are as similar as possible for different nanocrystals. An earlier report by some of us[16] demonstrated effective methods for the immobilization of alkanethiol-passivated gold nanocrystals using a xylenedithiol self-assembled monolayer. Figure 1 depicts a possible bonding geometry proposed to explain the results of that work, and those from subsequent experiments.[17] Using this method of immobilization, we demonstrate that nanocrystals of different mass can be accurately identified by their STM heights, despite impediments such as the weak dependence on mass (height $\propto M^{1/3}$) and the deformable ligand shell. We report separately on the tunneling spectra (STS).[18]

2. Experimental Section

Hexanethiolate-capped gold nanocrystals were prepared by reduction of gold−thiolate polymer compounds in a biphase reaction medium[2] similar to that developed by Brust and co-workers.[19] The resulting mixture of nanocrystal sizes was characterized by laser desorption ionization mass spectrometry (LDI-MS). In a custom-built time-of-flight mass spectrometer, negative ions were generated by irradiating neat films on stainless steel (1 μL of 10 mg/mL solution in toluene deposited) with a frequency tripled Nd:YAG laser (355 nm). Times of flight for laser-desorbed negative ions were mass calibrated using

[†] School of Chemistry, Georgia Institute of Technology.
[‡] Present address: James Franck Institute, University of Chicago, Chicago, IL.
[§] Oak Ridge National Laboratory.
[∥] School of Physics, Georgia Institute of Technology.
[⊥] Present address: Physics Dept., U.S. Military Academy, West Point, NY 10996.

10.1021/jp0376931 CCC: $27.50
Published on Web 03/02/2004

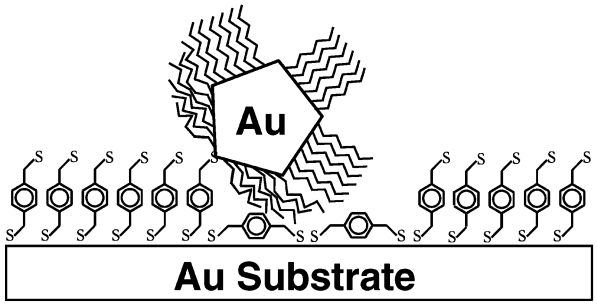

Figure 1. Schematic illustration of structural features discussed herein for a hexanethiol-passivated gold nanocrystal (pentagon) immobilized at a Au(111) substrate by means of a self-assembled monolayer (SAM) of xylenedithiol linkers.[16,17] Zigzag lines represent alkane chains; sulfur atoms at the Au nanocrystal facets are not shown. Note that spreading of the alkane chains could allow the nanocrystal to lie much closer to the substrate surface over the "lying-down" region of the SAM.

protein standards (e.g., ubiquitin, myoglobin, bovine serum albumin). Previous studies have shown that high-mass ions produced from neat films of gold-thiolate nanocrystals are consistent with the mass of the inorganic core of the nanocrystal compound (i.e., devoid of original hydrocarbon content).[20,21]

For STM, Au(111) substrates were prepared by vapor deposition of 120−150 nm Au films onto vacuum-baked mica at 450 °C.[22] After evaporation, the Au substrates were transferred to an ultrahigh vacuum (UHV) chamber to be cleaned by cycles of sputtering (500 eV Ne ions) and annealing (15 min at 420 °C) until a clear hexagonal low-energy electron diffraction (LEED) pattern was obtained (usually a single cycle was sufficient). STM images of Au(111) surfaces prepared in this manner routinely showed atomically flat terraces and the $22\times\sqrt{3}$ herringbone reconstruction.

Substrates were removed from the UHV chamber and transferred immediately to a 1 μM solution of 1,4-benzenedimethanethiol (xylenedithiol, XDT) in tetrahydrofuran (THF), remaining submerged for 1 h. When removed from the solution, substrates were rinsed thoroughly with a liberal amount of THF to remove any excess XDT. After drying under ambient conditions, the nanocrystals were deposited from a toluene solution (30 μg/mL). Typically, 10 μL of the solution was deposited on a 7 × 7 mm^2 surface placed under a cover glass in saturated toluene vapor to effect slow evaporation of the solvent (∼15 min). After drying, the surface was thoroughly rinsed with toluene to remove any unbound nanocrystals.[16]

Samples were imaged under ultrahigh vacuum conditions in a room-temperature STM system.[23] Electrochemically etched tungsten tips were cleaned by electron-bombardment heating prior to use. Samples were not treated or cleaned in any way once they were under vacuum. STM images for this work were acquired at a constant current of 100 pA, with a bias of −1 V applied to the tip. The sample was maintained at ground potential through the current preamplifier.

3. Results

The mass spectrum shown in Figure 2 is typical for a mixture of nanocrystal compounds produced by reduction of the gold-thiolate polymers.[2] The increased ion abundances centered at ca. 8, 14, 22, 29, and 34 kDa (1 kDa = 1.66 × 10^{-21} g) have been shown previously to correspond to the approximate mass of the inorganic core of the nanocrystal compounds, which can be separated by chemical methods[1,20] (peak widths are much larger than the mass resolution, $\Delta M/M \sim 10^{-3}$). Mass spectrometrically measured ion abundances generally reflect the relative

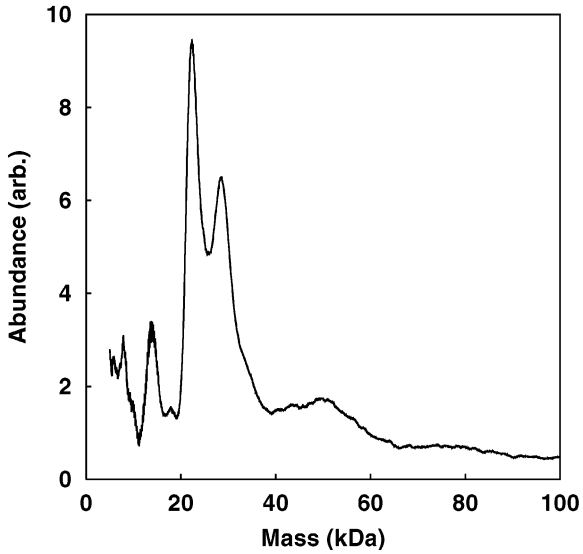

Figure 2. Laser desorption ionization mass spectrum obtained from a preparation of hexanethiol-capped gold nanocrystals. Note that the high-mass peaks (>40 kDa) include contributions from aggregation of the more abundant low-mass nanocrystals.[20]

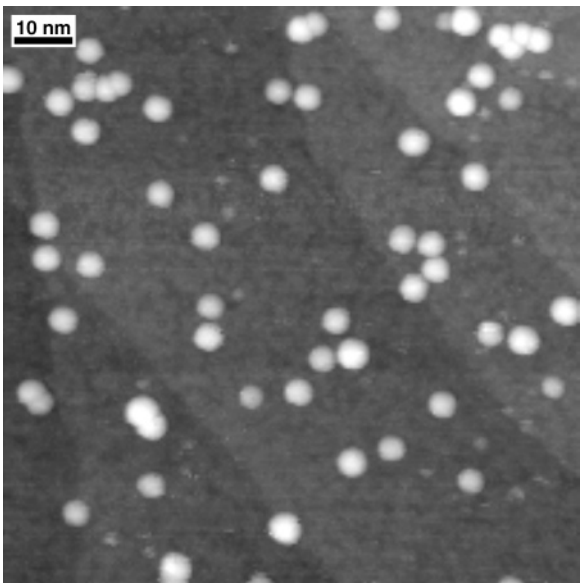

Figure 3. Room-temperature topographic image of mixed-size nanocrystals, 100 nm × 100 nm. Size differences are seen in both the apparent diameters and the heights. Surface height is displayed on a gray scale that spans 2.5 nm. Faint diagonal lines are steps in the Au(111) substrate. (tip voltage = −1.00 V, tunnel current = 100 pA.)

abundances of these nanocrystal compounds in the sample, although it should be noted that detector efficiency (i.e., ion-to-electron conversion) is somewhat larger for lower mass ions due to their higher velocity. Ion abundances above 40 kDa typically contain substantial contributions from gas-phase clustering of ions derived from smaller nanocrystals during the desorption/ionization process. In particular, the broad peak centered at 50 kDa has been shown to consist of ions generated from two distinct nanocrystal species with 45 and 55 kDa core mass.[20]

Figure 3 shows a room-temperature STM topograph of gold nanocrystals on Au(111). Differences in lateral diameter can be easily discerned in the distribution of nanocrystals, and relative height differences (brightness) are also apparent. The nanocrystal coverage shown in the image was typical of this sample, although some regions were found with large monolayer

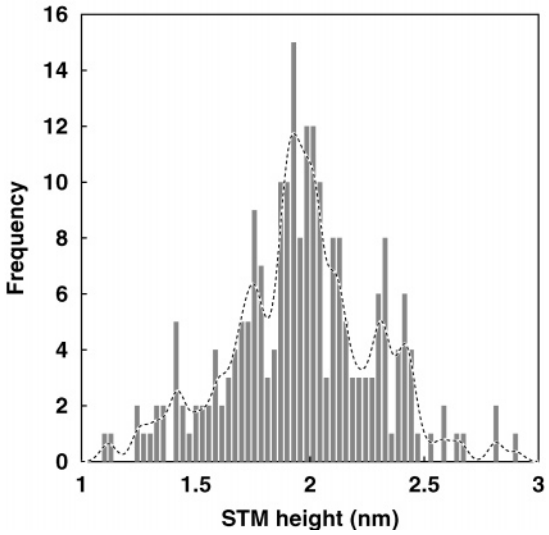

Figure 4. Frequencies of heights measured from STM profiles across 221 individual nanocrystals. Vertical bars: histogram obtained with a bin width of 0.028 nm. Dashed line: histogram bin width of 0.001 nm, convolved with a Gaussian (fwhm = 0.08 nm), and normalized to same area as the first histogram.

islands of nanocrystals. Despite thoroughly rinsing the sample with toluene, a nanocrystal would occasionally be dragged across the surface by the tip during imaging, appearing as a streak in the image.[16] Periodic spectroscopy over the clean surface verified that the tip itself was free of nanocrystals. In nanocrystal-free regions, Figure 3 shows monolayer-high atomic steps in the Au(111) surface beneath the SAM, as verified by their height of 0.24 nm. The image also shows many small depressions 0.1−0.2 nm deep.

To quantify the observed distribution of nanocrystal sizes, measured STM heights were tabulated for 221 different nanocrystals. Height was chosen as a measure of size instead of the apparent lateral diameter, because the tip shape affects the measured diameter but not the maximum height. Only regions similar to that pictured in Figure 3 were used for the analysis (i.e., no nanocrystal islands) because it was necessary to image the substrate near a nanocrystal for accurate height measurement. Height was always determined from profiles across the nanocrystal center and referenced to the lowest point on the SAM adjacent to the nanocrystal, but on the same scan line. These measurements were performed after a best-fit plane was subtracted from the entire image. Figure 4 shows two presentations of the resulting frequency of observed STM heights. Vertical bars are a simple histogram (bin width 0.028 nm), with the particle count N given on the vertical axis ($\pm\sqrt{N}$ statistical uncertainty for each peak). A more continuous representation of the data was obtained by convolving a finely binned histogram (0.001 nm bin width) with a Gaussian function [0.08 nm full-width-at-half-maximum (fwhm)], as shown by the dashed line in Figure 4 (after normalizing areas). The smoothing also reduces the statistical uncertainty at any point on the line to $\pm 0.6\ \sqrt{N}$ (at the expense of height resolution). Even considering uncertainties, the STM height histogram shows enhanced size populations at several heights, similar to the enhanced ion abundances measured by LDI mass spectrometry.

4. Discussion

SAM Configuration. In nanocrystal-free regions, Figure 3 shows atomic steps in the Au(111) surface beneath the SAM but also shows many irregular depressions 0.1−0.2 nm deep. In this work the SAM was intentionally allowed to form over only 1 h, much less than the time required for a dense monolayer.[24] We believe that the observed topography is due to two different phases of the xylenedithiol SAM, the depressions representing regions where the XDT has bound parallel to the surface in a "bidentate" fashion, as depicted in Figure 1. At saturation coverage, XDT has been found to bind to Ag surfaces in this parallel orientation whereas on gold surfaces it binds vertically.[25] If the coverage is reduced, however, XDT can bind to Au surfaces in the same parallel orientation as on Ag.[26,27] In fact, XDT on Au has been found to change from the upright to an approximately lying down position as it is heated beyond 100 °C.[25] This structural evolution is presumably the opposite of SAM formation wherein molecules first adsorb to form a low-density lying-down phase followed by conversion to a high-density upright phase as more molecules are added.[28]

Although prior STM studies of adsorbed xylenes exist,[29−31] none are appropriate for determining the imaged height difference between XDT monolayer phases (i.e., lying down vs standing up). Consequently, we will estimate the height difference by comparison with a well-studied thiolate self-assembled monolayer system: 1,6-mercaptohexanol.[28] The physical size of 1,6-mercaptohexanol is about 1 nm long[28] and about 0.5 nm in diameter, estimated from nearest-neighbor close packing of *n*-alkanethiols.[32] The STM-imaged heights of mercaptohexanol were about 0.1 nm lying down[28,33] and about 0.18 nm in the upright position.[28] Because the XDT is presumably more sterically hindered than mercaptohexanol, the difference in standing up vs lying down phases (0.08 nm) in mercaptohexanol layers likely sets a lower limit for the XDT monolayers, consistent with the ∼0.1 nm depressions observed in Figure 3. Local density of states differences could also account for a portion of the measured height difference.

Based on these structural and STM-imaged height arguments, the topography observed in Figure 3 is consistent with a biphasic monolayer, as can be achieved by limiting the incubation time of the film.[28] In fact, phase boundaries in such a dithiol SAM may relieve steric constraints that would otherwise impede nanocrystal binding on close-packed monolayers (see Figure 1).

STM-Height/Core-Mass Correlation. The observed similarities in the measured mass and height distributions of the nanocrystal compounds suggest a more direct comparison. Translation between these two disparate measures of physical dimension depends on many different factors (LDI-MS desorption products, electronic structure, ligand conformation, variations in bonding geometry, etc.), and the relative contribution of each is not yet known.

Using a spherical core approximation and the bulk density of gold, the effective core diameter $2R$ is obtained from the measured mass M as

$$2R\ [\mathrm{nm}] = 0.548 \times (M\ [\mathrm{kDa}])^{1/3}$$

which allows a direct comparison with the STM heights. The correlation between STM height h and core mass then becomes apparent, as shown in Figure 5. Here the LDI-MS spectrum has been plotted versus effective nanocrystal core diameter[34] and the STM height histogram has been overlaid after offsetting the height axis by −0.36 nm so as to align the major abundance peaks in the two distributions.

Figure 5 establishes a clear correspondence between the histogram peaks and all 6 mass peaks (treating 45 and 55 kDa as a single broad peak). The peak positions and relative abundances are both very similar in the two measurements.[35]

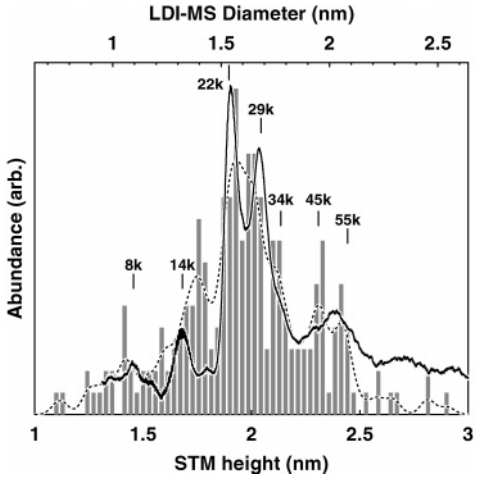

Figure 5. Histogram of measured STM heights (vertical bars and dashed line; see Figure 4) plotted with LDI time-of-flight mass spectrum (solid line) of the same nanocrystal mixture. Mass abundance is plotted versus mean core diameter (top scale), derived from the measured masses assuming a spherical particle and bulk density. Top and bottom scales are offset 0.36 nm to align abundance peaks.

This result has several implications: (1) The adsorption of nanocrystals was essentially independent of mass, from 8 to 55 kDa. (2) Height variations due to different adsorption geometries or nanocrystal orientations were small. (3) The measurement method sufficiently accounted for the intrinsic SAM topographic variations. (4) The contribution of the ligand shell was nearly independent of nanocrystal size. (5) The effect of size-dependent electronic structure on the measured heights was generally small. (6) The adsorbed nanocrystal cores must have been essentially undeformed from their prepared state.

Some of these effects may still contribute to the detailed shape of the histogram by broadening or shifting the peaks. For example, the hexanethiol bound to the nanocrystals is expected to be above its chain disordering ("melting") temperature at room temperature.[36] The ligand shell could then deform and contribute to the broadening of histogram peaks. The SAM topography can also provide opportunities for different adsorption geometries that would broaden the histogram peaks.

The poorest correlation is found for the 14 kDa mass peak. For the smallest masses (8, 14 kDa) the peak positions could be influenced by changes in nanocrystal electronic structure, because the tunneling energy gap is larger for smaller nanocrystals.[13,18] Also, some of the proposed structures[7,8] are far from the spherical approximation employed here, thus preferential adsorption of nanocrystals on a particular facet (or edge) could shift the peak position. For example, the calculated diameter of a truncated-octahedral face-centered-cubic $Au_{38}(SCH_3)_{24}$ nanocrystal structure[10] was 1.13 nm in the (100) direction and 1.02 nm in the (111) direction.[37] The maximum observed deviation between STM-height and core-diameter peak positions is 0.07 nm (14 kDa peak), which we will ultimately take to be the maximum uncertainty in the determination of mean core diameter from STM height in this size range.

Figure 6 shows a simplified schematic of the STM trajectory over a nanocrystal bound to the SAM. The measured STM height h depends on the nanocrystal core diameter $2R$ and other factors such as the bonding geometry (including interpenetration of the SAM and ligand layers), the ligand conformation (e.g., ordered vs disordered), and changes in the local density-of-states from SAM/substrate to ligand/nanocrystal. Any or all of these could be different for different nanocrystal species. In the schematic we define a parameter $\Delta = h - 2R$ that depends on

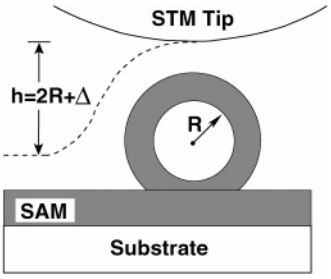

Figure 6. Schematic of STM tip trajectory (dashed line) over a nanocrystal of core radius R. The measured STM height is h. The shift $\Delta = h - 2R$ is obtained by aligning the STM height histogram and the distribution of core diameters determined by LDI-MS (see Figure 5). Strong correlation between abundance peaks in these distributions shows that Δ remains constant throughout most of the size range studied here. Consequently, the binding geometry and tunnel gap must be similar for different nanocrystals.

these factors but is independent of core size. The fact that a constant value of Δ effectively maps abundance peaks in the height histogram to those in the LDI-MS distribution of core diameters shows that the listed factors are nearly independent of nanocrystal species within the size range studied.

To further quantify Δ, we note that in Figure 5 the height histogram was shifted to best represent the correlation with relative abundance peaks in the mass spectrum. However, the nanocrystal core mass (and mass-derived core diameter) should be obtained from the *leading edge* of the LDI-MS peak, as argued in previous work[20] and recently elaborated.[21] Making this association gives a difference of $\Delta = 0.38$ nm between the most abundant nanocrystal height measured by STM and its mass-derived core diameter.

If we make the simple assumption that the tip−core and tip−SAM separations are equal, then Δ provides an estimate of the core−substrate separation. The observed Δ is smaller than would be expected for the core−surface separation of a hexanethiol-passivated Au nanocrystal sitting on a xylenedithiol SAM. First, the core−surface separation must include the physical height of the SAM. The high-density (standing up) phase of the XDT SAM on Au(111) is expected to be 0.92 nm thick but was measured by ellipsometry to be 0.83 nm thick.[38] Alternatively, the low-density (lying down) phase of the XDT SAM on Ag(111) is expected to be about 0.47 nm thick.[25] Second, the core−surface separation must include the ligand shell. The nanocrystals are coated with a monolayer of hexanethiol (length: 0.84 nm), further inhibiting their approach toward the surface. Nanocrystal array measurements, however, show that hexanethiol-passivated 29 kDa nanocrystals pack such that their cores are separated by only 1.0 nm,[39] i.e., less than twice the ligand length. This small separation is attributed to interpenetration of the alkane chains.[36,39,40] On a flat surface, simulations show that longer chain thiols tend to spread away from edges and corners of the Au core, facilitating core−surface separations as small as 0.58 nm for dodecanethiol.[36] The effects of parting the thiol chains and interpenetration of the SAM may combine to greatly reduce the core−surface separation. On the basis of these considerations, we propose that a typical binding geometry could be as shown schematically in Figure 1. This would give a small core−substrate separation and would allow easy penetration of the alkanethiol ligand layer. Even so, the measured value of Δ is smaller than the nanocrystal−surface separation expected from this model geometry.

The remaining discrepancy between Δ and the geometric nanocrystal−surface distance (at least 0.1 nm) is most likely due to the inadequacy of our assumption of equal tip−surface

and tip−core distances. Voltage division between the two tunnel junctions (tip−nanocrystal and nanocrystal−substrate), density-of-states changes, and the differing electronic structures of the SAM and adsorbed ligand layer could all decrease the imaged heights. These issues remain to be clarified, but the correspondence of peaks between the STM height histogram and the mass abundances demonstrates that *variations* in Δ are small for nanocrystals from 8 to 55 kDa.

Mass-Resolved STM Measurements. The height−mass correlation is an extremely valuable tool for STM experiments. It is now possible to make size-dependent electronic property studies as a function of the *core* radius or *core mass* of each individual nanocrystal. This is quite distinct from spectroscopic measurements on poorly characterized metal particles for two reasons: (1) spectra can be related to other single-molecule measurements; (2) spectra from single nanocrystals can be correlated with macroscopic ensemble measurements of each nanocrystal species. The importance of identifying the nanocrystals is underscored by considering the difficulty of perfectly separating these species from one another.[1,2] Furthermore, spectroscopic measurements can be done on a variety of nanocrystal masses without changing samples, and therefore without changing the tunneling conditions (as would typically occur if one had to switch samples entirely). At cryogenic temperatures, we have found the tunneling parameters to be sensitive to the geometry of the junction,[15] which is partially determined by the shape of the tip. Additionally, low temperature measurements provide many challenges, so making all measurements on a single sample is highly advantageous. Note that the height−mass correlation should be repeated at the measurement temperature because the ligand layer may undergo a phase transition that would change the offset (Δ) of the STM- and mass-derived size distributions.[36]

5. Conclusion

We have shown that gold nanocrystals of different masses can be positively identified in scanning tunneling microscopy experiments by comparing the height distribution measured by STM with the core size distribution measured directly by mass spectrometry. A histogram of nanocrystal heights revealed several peaks that correlate well with distinct peaks in the mass spectrum. This establishes a mapping between STM height and nanocrystal core diameter or core mass. The map will enable the compilation of single molecule spectra for each nanocrystal species and will facilitate comparisons to ensemble measurements.

Acknowledgment. We thank Dr. W. G. Cullen for advice and assistance. This work was supported in part by grants from the U.S. National Science Foundation (DMR-9632780 and CHE-9700562) and the Department of Energy (DE-FG02-02ER45956). Research at Oak Ridge National Laboratory supported by the Division of Materials Sciences, Office of Basic Energy Sciences, U.S .Department of Energy. Oak Ridge National Laboratory is managed and operated by UT-Battelle, LLC, under contract DE-AC05-00OR22725

References and Notes

(1) Whetten, R. L.; Khoury, J. T.; Alvarez, M. M.; Murthy, S.; Vezmar, I.; Wang, Z. L.; Stephens, P. W.; Cleveland, C. L.; Luedtke, W. D.; Landman, U. *Adv. Mater.* **1996**, *8*, 428−434.

(2) Schaaff, T. G.; Shafigullin, M. N.; Khoury, J. T.; Vezmar, I.; Whetten, R. L.; Cullen, W. G.; First, P. N.; Gutierrez-Wing, C.; Ascensio, J.; Jose-Yacaman, M. J. *J. Phys. Chem. B* **1997**, *101*, 7885−7891.

(3) Martin, T. P.; Bergmann, T.; Gohlich, H.; Lange, T. *J. Phys. Chem.* **1991**, *95*, 6421−6429.

(4) Taylor, L. J.; Pettiette-Hall, C. L.; Cheshnovsky, O.; Smalley, R. E. *J. Chem. Phys.* **1992**, *96*, 3319−3329.

(5) Martin, T. P. *Phys. Rep.* **1996**, *273*, 199−241.

(6) Cleveland, C. L.; Landman, U.; Shafigullin, M. N.; Stephens, P. W.; Whetten, R. L. *Z. Phys. D* **1997**, *40*, 503−508.

(7) Cleveland, C. L.; Landman, U.; Schaaff, T. G.; Shafigullin, M. N.; Stephens, P. W.; Whetten, R. L. *Phys. Rev. Lett.* **1997**, *79*, 1873−1876.

(8) Shafigullin, M. N. Preparation and structural studies of gold nanocrystals and their arrays. Thesis, Georgia Institute of Technology, 1999.

(9) Haberlen, O. D.; Chung, S. C.; Stener, M.; Rösch, N. R. *Bunsen-Ges. Phys. Chem.* **1997**, *106*, 5189−5198.

(10) Hakkinen, H.; Barnett, R.; Landman, U. *Phys. Rev. Lett.* **1999**, *82*, 3264−3267.

(11) Dabbousi, B. O.; RodriguezViejo, J.; Mikulec, F. V.; Heine, J. R.; Mattoussi, H.; Ober, R.; Jensen, K. F.; Bawendi, M. G. *J. Phys. Chem. B* **1997**, *101*, 9463−9475.

(12) Banin, U.; Cao, Y.; Katz, D.; Millo, O. *Nature* **1999**, *400*, 542−544.

(13) Wang, B.; Wang, H. Q.; Li, H. X.; Zeng, C. G.; Hou, J. G.; Xiao, X. D. *Phys. Rev. B* **2001**, *63*, art. no.-035403.

(14) Chen, S.; Ingram, R. S.; Hostetler, M. J.; Pietron, J. J.; Murray, R. W.; Schaaff, T. G.; Khoury, J. T.; Alvarez, M. M.; Whetten, R. L. *Science* **1998**, *280*, 2098−2101.

(15) Bigioni, T. P.; Harrell, L. E.; Cullen, W. G.; Guthrie, D. K.; Whetten, R. L.; First, P. N. *Eur. Phys. J. D* **1999**, *6*, 355−364.

(16) Harrell, L. E.; Bigioni, T. P.; Cullen, W. G.; Whetten, R. L.; First, P. N. *J. Vac. Sci. Technol. B* **1999**, *17*, 2411−2416.

(17) Bigioni, T. P. Scanning tunneling microscopy and spectroscopy of passivated gold nanocrystals. Thesis, Georgia Institute of Technology, 2000.

(18) Bigioni, T. P.; Schaaff, T. G.; Whetten, R. L.; First, P. N. To be published.

(19) Brust, M.; Walker, M.; Bethell, D.; Schiffrin, D. J.; Whyman, R. *Chem. Commun.* **1994**, 801−802.

(20) Vezmar, I.; Alvarez, M. M.; Khoury, J. T.; Salisbury, B. E.; Shafigullin, M. N. *Z. Phys. D* **1997**, *40*, 147−151.

(21) Schaaff, T. G. Submitted to *Anal. Chem.*

(22) DeRose, J. A.; Thundat, T.; Nagahara, L. A.; Lindsay, S. M. *Surf. Sci.* **1991**, *256*, 102−108.

(23) Quesenberry, P. E.; First, P. N. *Phys. Rev. B* **1996**, *54*, 8218−8230.

(24) Andres, R. P.; Datta, S.; Dorogi, M.; Gomez, J.; Henderson, J. I.; Janes, D. B.; Kolagunta, V. R.; Kubiak, C. P.; Mahoney, W.; Osifchin, R. F.; Reifenberger, R.; Samanta, M. P.; Tian, W. *J. Vac. Sci. Technol. A* **1996**, *14*, 1178−1183.

(25) Murty, K. V. G. K.; Venkataramanan, M.; Pradeep, T. *Langmuir* **1998**, *14*, 5446−5456.

(26) Joo, S. W.; Han, S. W.; Kim, K. *J. Phys. Chem. B* **1999**, *103*, 10831−10837.

(27) Venkataramanan, M.; Pradeep, T. *Anal. Chem.* **2000**, *72*, 5852−5856.

(28) Poirier, G. E.; Pylant, E. D. *Science* **1996**, *272*, 1145−1148.

(29) Futaba, D. N.; Landry, J. P.; Loui, A.; Chiang, S. *J. Vac. Sci. Technol. A* **2001**, *19*, 1993−1995.

(30) Suto, K.; Wakisaka, M.; Yamagishi, M.; Wan, L. J.; Inukai, J.; Itaya, K. *Langmuir* **2000**, *16*, 9368−9373.

(31) Cernota, P. D.; Yoon, H. A.; Salmeron, M.; Somorjai, G. A. *Surf. Sci.* **1998**, *415*, 351−362.

(32) Poirier, G. E.; Tarlov, M. J. *Langmuir* **1994**, *10*, 2853−2856.

(33) Cyr, D. M.; Venkataraman, B.; Flynn, G. W.; Black, A.; Whitesides, G. M. *J. Phys. Chem.* **1996**, *100*, 13747−13759.

(34) Note that transformation of the independent variable from M to $2R$ requires a Jacobian factor $dM/dR \propto R^2$, which affects the LDI-MS peak heights.

(35) Considering the statistical uncertainties, one might argue that only three peaks are actually resolved in the STM height histogram: 14 kDa, 22 + 29 + 34 kDa, and 45 + 55 kDa. The excellent correlation with *six* mass abundance peaks provides further evidence that the nanocrystal preparation results in distinct chemical species, with many fewer nanocrystals between these stable core sizes. Ultimately, the mapping from STM height to nanocrystal core diameter will not be strongly dependent on whether one assumes 3 distinct peaks or more, but these structures allow accurate correlation of the two size measurements and lend confidence that STM height measurements can distinguish the different nanocrystal species.

(36) Luedtke, W. D.; Landman, U. *J. Phys. Chem.* **1996**, *100*, 13323−13329.

(37) Hakkinen, H.; Barnett, R. N.; Landman, U. Private communication.

(38) Henderson, J. I.; Feng, S.; Ferrence, G. M.; Bein, T.; Kubiak, C. P. *Inorg. Chim. Acta* **1996**, *242*, 115−124.

(39) Whetten, R. L.; Shafigullin, M. N.; Khoury, J. T.; Schaaff, T. G.; Vezmar, I.; Alvarez, M. M.; Wilkinson, A. *Acc. Chem. Res.* **1999**, *32*, 397−406.

(40) Wang, Z. L.; Harfenist, S. A.; Vezmar, I.; Whetten, R. L.; Bentley, J.; Evans, N. D.; Alexander, K. B. *Adv. Mater.* **1998**, *10*, 808−812.